ESTIMATING FOREST PARAMETERS FROM TOP-OF-ATMOSPHERE RADIANCE MEASUREMENTS USING COUPLED RADIATIVE TRANSFER MODELS

Valérie Laurent[(1)], Wout Verhoef[(2)], Jan Clevers[(1)], Michael Schaepman[(3)]

[(1)] Centre for Geo-Information, Wageningen University, P.O. Box 47, 6700 AA Wageningen, the Netherlands, Email: Valerie.Laurent@wur.nl, Jan.Clevers@wur.nl
[(2)] Faculty of Geo-Information Science and Earth Observation (ITC), University of Twente, P.O. Box 6, 7500 AA Enschede, the Netherlands, Email: Verhoef@itc.nl
[(3)] RSL, Department of Geography, University of Zurich – Irchel, Winterthurerstr. 190, CH-8057 Zurich, Switzerland, Email: Michael.Schaepman@geo.uzh.ch

ABSTRACT

The canopy and atmosphere radiative transfer models SLC and MODTRAN were coupled to simulate top-of-atmosphere (TOA) radiance data for 3 Norway spruce stands in Eastern Czech Republic. The simulations fitted the near-nadir CHRIS radiance data well. A sensitivity analysis based on the singular value decomposition of the Jacobian matrix provided useful information for building the look up tables needed to estimate needle and canopy parameters. Canopy cover, fraction of bark in the plant area index, needle chlorophyll and dry matter content were estimated using the TOA CHRIS radiance. For comparison, the simulations, sensitivity analysis and parameter estimations were also conducted for the top of canopy (TOC) level, using atmospherically corrected CHRIS reflectance data. The results showed that the TOA approach performs as good as the TOC approach and allowed decreasing the ill-posedness for at least one stand.

1. INTRODUCTION

Forests are important ecosystems on Earth: they cover about 30% of the land surface, provide a wide range of services and have a major role in the carbon cycle. Climate and biomass models therefore use a range of forest parameters (e.g. leaf area index, canopy cover, and chlorophyll content) as inputs. These parameters can be estimated and monitored thanks to the combined use of remote sensing data and physically-based radiative transfer (RT) models. Since RT models simulate the optical properties of the medium based on its physical properties, parameter estimation requires inverting the model. The inversion problem, however, is known to be ill-posed and under-determined. Several regularization methods have been proposed to reduce the ill-posedness [1]: using prior information, enforcing spatial and/or temporal constraints, and coupling models. This study focuses on the coupling method. Most studies couple soil, leaf and canopy models to simulate the top of canopy (TOC) reflectance and then compare the simulation output to remote sensing data, atmospherically corrected by inverting an atmosphere RT model. Using the same models as in this TOC approach, it is possible to achieve a higher degree of coupling, thus reducing the ill-posedness of the inversion [1]. Maximum coupling can be achieved by integrating the atmosphere model with the soil, leaf, and canopy models in the simulation set-up. Such a coupled model then simulates the top of atmosphere (TOA) radiance, thus eliminating the need for atmospheric correction. Using the atmospheric model in forward mode only allows including surface directional effects as well as topography effects. In addition, working at TOA level makes direct radiance data assimilation more practical [2].
This study used the SLC soil-leaf-canopy [3] and MODTRAN atmosphere [4] models to simulate and estimate canopy parameters for 3 Norway spruce stands in Eastern Czech Republic using TOA radiance near-nadir data measured by CHRIS (Compact High Resolution Imaging Spectrometer) on board of the PROBA (Project for On Board Autonomy) satellite platform. The results are compared to those obtained when working at TOC level with atmospherically corrected CHRIS reflectance data.

2. MATERIALS AND METHODS

The first 2 subsections present calculations which are valid for any 4-stream surface and atmosphere models.

2.1. TOA radiance simulation: surface – atmosphere coupling

In the 4-stream approximation of the surface-atmosphere radiative transfer, the TOA radiance in the observer direction L_o can be calculated as [5]:

$$L_o = \frac{E_s^o}{\pi}\cos\theta_s \left(\begin{array}{l} \rho_{so} + \dfrac{\tau_{ss}\overline{r_{sd}} + \tau_{sd}\overline{r_{dd}}}{1-\overline{r_{dd}}\rho_{dd}}\tau_{do} \\ + \dfrac{\tau_{sd} + \tau_{ss}\overline{r_{sd}}\rho_{dd}}{1-\overline{r_{dd}}\rho_{dd}} r_{do}\tau_{oo} \\ + \tau_{ss} r_{so}\tau_{oo} \end{array} \right) \qquad (1)$$

where E_s^o is the extraterrestrial solar irradiance on a plane perpendicular to the sunrays, θ_s the local solar zenith angle, ρ the reflectance of a layer through volume scattering, τ the transmittance through a layer, *r* the reflectance of a surface, *o* indicates the direction of observation, *s* the direction of the sunrays, *d* diffuse hemispherical radiation, and the over bars indicate low-pass spatial filtering over the surroundings of the target pixel to account for the adjacency effect. Following the approach in [6], which was originally developed to include also the thermal domain, Eq. 1 can be rewritten using the atmospheric path radiance L_{p0}, and a set of gain factors *G* as:

$$L_o = L_{p0} + \frac{G_{ssdo}\overline{r_{sd}} + G_{sddo}\overline{r_{dd}}}{1-\overline{r_{dd}}\rho_{dd}} + \frac{G_{sdoo} + G_{mult}\overline{r_{sd}}}{1-\overline{r_{dd}}\rho_{dd}} r_{do} + G_{ssoo} r_{so} \quad (2)$$

where

$$L_{p0} = \frac{E_s^o \cos\theta_s}{\pi}\rho_{so}, \qquad G_{ssoo} = \frac{E_s^o \cos\theta_s}{\pi}\tau_{ss}\tau_{oo},$$

$$G_{ssdo} = \frac{E_s^o \cos\theta_s}{\pi}\tau_{ss}\tau_{do}, \quad G_{sddo} = \frac{E_s^o \cos\theta_s}{\pi}\tau_{sd}\tau_{do},$$

$$G_{sdoo} = \frac{E_s^o \cos\theta_s}{\pi}\tau_{sd}\tau_{oo}, \quad G_{mult} = \frac{E_s^o \cos\theta_s}{\pi}\tau_{ss}\rho_{dd}\tau_{oo}.$$

The 7 parameters in Eq. 2 can be calculated using any atmospheric model having the total path radiance (PATH), the sunlight ground-reflected radiance (GSUN) and the total ground-reflected radiance (GTOT) in its outputs. Only 3 model runs for Lambertian surfaces of different albedo values are needed. Using subscripts 0, 50, or 100 to indicate albedo values of 0, 0.5, or 1, it can be verified that the parameters can be calculated as follows:

$$L_{p0} = PATH_0 \quad (3)$$

$$G_{ssoo} = GSUN_{100} \quad (4)$$

$$\rho_{dd} = \frac{GTOT_{100} - 2GTOT_{50}}{GTOT_{100} - GTOT_{50}} \quad (5)$$

$$G_{mult} = \rho_{dd} GSUN_{100} \quad (6)$$

$$G_{sdoo} = (1-\rho_{dd})GTOT_{100} - GSUN_{100} \quad (7)$$

$$G_{sddo} = \frac{PATH_{100} - PATH_0}{GTOT_{100}} G_{sdoo} \quad (8)$$

$$G_{ssdo} = \frac{PATH_{100} - PATH_0}{GTOT_{100}} GSUN_{100} \quad (9)$$

2.2. Atmospheric correction

As mentioned in the introduction, atmospheric correction is an inverse problem. In Eq. 2, there are 4 unknowns, the 4 surface reflectances, which causes the atmospheric correction problem to be underdetermined. To decrease the number of unknowns, it is necessary to assume that both target and background are Lambertian, so in this case: $r_{so} = r_{do} = r_t$ and $r_{sd} = r_{dd} = r_b$. Exploiting the low-pass filtered radiance in the observer's direction $\overline{L_o}$ gives a 2nd equation, allowing solving for r_t and r_b. In particular, r_t can be calculated as:

$$r_t = \frac{L_o - L_{p0} + \frac{G_b}{G_t}\left(L_o - \overline{L_o}\right)}{G_b + G_t + \rho_{dd}(\overline{L_o} - L_{p0})} \quad (10)$$

where $G_t = G_{sdoo} + G_{ssoo}$, and $G_b = G_{ssdo} + G_{sddo}$.

2.3. Study area and data

The study area is located in Eastern Czech Republic, at the Bily Kriz experimental research site in the Moravian-Silesian Beskydy Mountains, (18.54°E, 49.50°N, altitude 936 m above sea level). A detailed description of the environmental conditions can be found in [7]. The forest area is dominated by montane Norway spruce (*Picea abies* (L.) Karst.). Three stands of different ages and structures were selected for the study (Tab. 1). The field data were collected in the first half of September 2006 as part of the HYPERTREES (HYPERspectral ThREE scales) field/flight campaign.

The main remote sensing data was a near-nadir image acquired on September 12th, 2006, by CHRIS/PROBA. The image was acquired in chlorophyll mode (mode 4), resulting in 18 spectral bands in the range 485-802 nm at a spatial resolution of 17 m, with the geometry described in Tab. 2. The CHRIS image was radiometrically calibrated by the data provider and was further de-striped, geo-corrected and ortho-rectified using Toussin's approach and nearest neighbour interpolation [8].

Table 2. Acquisition geometry of the CHRIS image

SZA	SAA	VZA	VAA
46.6	162.7	16.0	138.1

An AISA (Airborne Imaging Spectro-radiometer for Applications) Eagle image acquired on September 14th, 2006 was also available. It had 40 spectral bands in the range 450-830 nm and a spatial resolution of 40 cm. The AISA image was radiometrically calibrated, geo-corrected, ortho-rectified, and atmospherically corrected using the ATCOR4 software [8].

In MODTRAN, the urban aerosol type was chosen because there is an urban-industrial zone located 20 km north of the study and north wind is dominant in the area. In addition, higher air concentrations of SO_2 were recorded at the study area on the day of AISA acquisition [8]. The visibility (vis) was chosen as the smallest value allowing all radiances in the CHRIS image to be higher than the simulated atmospheric path radiance L_{p0}. The surface height (height) was 936 m, the surface temperature (stemp) was set to 20°C, and the default ozone (O_3) and water vapour (H_2O) columns were used.

Canopy structure measurements (Tab. 1) included tree height, crown radius, and length of live and dead crown, all measured with a laser rangefinder Impulse 200. The canopy cover (Cv) was estimated by classifying an AISA image [9]. The plant area index (PAI), defined as half of the total plant area (needles and non photosynthetic plant material) per unit of ground surface area [10], was estimated in each stand by 3 methods: a systematic sampling grid of 10 m cells was used for the LAI-2000 plant canopy analyzer and hemispherical photographs methods whereas the TRAC (Tracing Radiation and Architecture of Canopies) method required using transects [11]. The obtained values were averaged to get one PAI value for each stand. The fraction of woody material fB (mainly bark) in the PAI for YOUNG was taken from the destructive sampling study of [12].

Table 1. Stand characteristics and model inputs

Stand		YOUNG	OLD1	OLD2
Age (years)		29	100	75
Density (trees/ha)		1450	160	420
DBH (cm)		14	53	37
# CHRIS pixels		4	13	10
Canopy	PAI	8.88	5.73	7.35
	fB	0.13	0.23	0.4
	D	0.4	0.4	0.1
	Hot	0.01	0.01	0.01
	LDF	Spherical	Spherical	Spherical
	Cv	0.9	0.55	0.7
	Z	0.34	0.24	0.26
Needle	Cab (µg/cm^2)	55	60	65
	Cw (cm)	0.02	0.02	0.02
	Cdm (g/cm^2)	0.04	0.04	0.04
	Cs	0	0	0
	N	1.8	1.7	1.7
Bark	Cab (µg/cm^2)	10		
	Cw (cm)	0		
	Cdm (g/cm^2)	0.5		
	Cs	15		
	N	10		

The needle spectral measurements were carried out on 10 sample trees in the YOUNG stand and 20 in the OLD1 stand. Needles were sampled in a stratified way according to irradiation regime and age. From each sample tree, one branch was cut in each of the sunlit, shaded and intermediate irradiation zones. Then, from each branch, sets of needles of the current year and of 1, 2, and 3 year-old were collected. The optical properties of each needle set were measured at 1 nm resolution with an ASD spectro-radiometer coupled with a Li-Cor integrating sphere, and corrected for the gap fraction between the needles on the carrier.

The spectral properties of the main soil components, understory species and bark were measured in the field at 1 nm resolution with an ASD spectro-radiometer. The background signature was calculated as a weighted average of the main soil and understory components. The background of the YOUNG stand was a mixture of litter, humus, and soil, whereas the background of the OLD1 and OLD2 stands consisted of a majority of blueberry, blackberry, and grass.

2.4. Radiative transfer models and settings used

The Soil-Leaf-Canopy (SLC) model [3] was used to simulate the (TOC) reflectance of the stands. It couples:

- 4SOIL: soil reflectance model which was not used in this study,
- PROSPECT: leaf reflectance model [13], modified to include brown pigments (Cs) [5]. Since PROSPECT does not work well for needles [14], it was optimized to match the measured optical data. It was also parameterized to simulate the bark.
- 4SAIL2: canopy reflectance model which includes the crown clumping effect thanks to the introduction of two additional inputs: crown cover (Cv) and tree shape factor (Zeta) defined as the crown diameter divided by the height of the crown centre above ground. 4SAIL2 allows mixing green and brown leaves in the canopy [3]. The brown leaves feature was used for the bark.

The MODTRAN 4.1 model [4] was used for the atmosphere. The following options were selected: DISORT algorithm with 8 streams, medium speed correlated-k option with 17 values, and 5 cm^{-1} database.

The TOC reflectances and the MODTRAN outputs were resampled to the CHRIS bands using Gaussian approximations of the sensor response functions. The adjacency effect was neglected, so Eq. 2 became:

$$L_o = L_{p0} + \frac{G_{ssdo} r_{sd} + G_{sddo} r_{dd}}{1 - r_{dd}\rho_{dd}} + \frac{G_{sdoo} + G_{mult} r_{sd}}{1 - r_{dd}\rho_{dd}} r_{do} + G_{ssoo} r_{so} \quad (11)$$

And Eq. 10 became:

$$r_t = \frac{L_o - L_{p0}}{G + \rho_{dd}(L_o - L_{p0})} \quad (12)$$

where $G = G_t + G_b$. The atmospheric gain factors were calculated from the MODTRAN outputs using Eq. 3-9 and the TOC reflectances were directly produced by SLC.

2.5. Problem dimensionality and local sensitivity analysis

For each stand and for both TOA and TOC levels, the Jacobian matrix **J** was built as follows: each input parameter was varied from its default value by 1% of its potential variation range, the model was run with the new parameter value, and the relative difference between the signatures produced by the new and default run was stored in a column of **J**. Thus,

$$\Delta\mathbf{r} = \mathbf{J}\Delta\mathbf{p} \quad (13)$$

Where $\Delta\mathbf{p}$ is the matrix of parameter variation for each parameter and $\Delta\mathbf{r}$ is the matrix of relative model output difference for each wavelength. Following [15], a singular value decomposition was then applied to **J**, yielding a factorization of **J**:

$$\mathbf{J} = \mathbf{U}\mathbf{S}\mathbf{V}^t \quad (14)$$

where **S** diagonal, and **U** and **V** orthonormal. In particular, **U** and **V** are orthogonal, so one can write: $\mathbf{U}^t\mathbf{U} = \mathbf{U}\mathbf{U}^t = \mathbf{I}$, and $\mathbf{V}^t\mathbf{V} = \mathbf{V}\mathbf{V}^t = \mathbf{I}$. Combining these and Eq. 13 and 14, one gets:

$$\mathbf{U}^t\Delta\mathbf{r} = \mathbf{S}\mathbf{V}^t\Delta\mathbf{p} \quad (15)$$

Eq. 15 expresses that there is a one-to-one relationship between the transformed model output differences $\mathbf{U}^t\Delta\mathbf{r}$ and the transformed parameter variations $\mathbf{V}^t\Delta\mathbf{p}$. The rank of **S** reflects the rank of the estimation problem, and the rows of the $\mathbf{V}^t$ matrix contain the loadings of the parameter variations onto the base of the transformed parameter variations space. The hotspot parameter was not included in the Jacobian matrix because it was very influential and masked the other parameters, and its value of 0.01 is well known for forest. Several atmosphere parameters (see section 2.3) were included in the SVD at TOA level in addition to the SLC input parameters.

2.6. Parameter estimation

Six look-up tables (LUT) were built for each stand and each level. Based on the SVD results (see section 3.2), the free parameters were: Cv, fB, needle Cab and needle Cdm (See Tab. 3). The TOC LUTs store the r_{so} signatures, and the TOA LUTs store the L_o signatures. Because of the irregular spectral coverage of the CHRIS spectral bands, the weighted root mean square difference (WRMSD) between the simulation and the measured CHRIS signature was used as the cost function. In case of multiple solutions, the average was taken for each parameter.

Table 3. Specifications of the LUT

Parameter	Min	Max	Step	#values
fB	0	1	0.1	11
Cv	0	1	0.1	11
Needle Cab (µg/cm^2)	0	100	5	21
Needle Cdm (g/cm^2)	0	0.05	0.005	11

3. RESULTS

3.1. Simulations

The result of the optimization of PROSPECT to simulate the bark material in the forest canopy is presented in Fig. 1. A good match with the measured reflectance could be achieved thanks to the presence of the brown pigments that were included in the model. The simulated transmittance was zero, as should be for bark material. As expected, the best agreement was obtained for high values of N, Cdm, and Cs, Cw=0, and low Cab. A small discrepancy persisted in the blue range from 500 to 550 nm. This may be due to chemical components not included in PROSPECT.

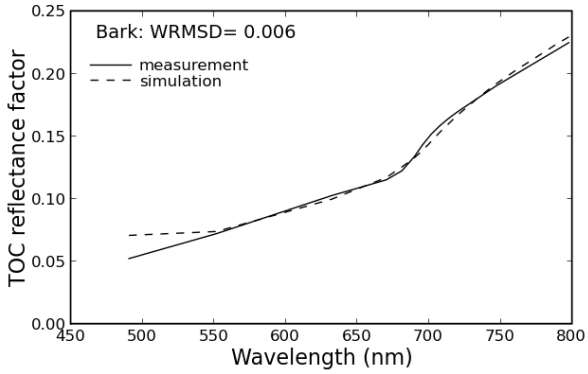

Figure 1. Measured and simulated bark reflectance factor

Regarding the needles, it was possible to obtain a good match between the PROSPECT simulations and the measured signatures for YOUNG and OLD1 (Fig. 2). No field measurements were available for OLD2, but one can note that the simulated reflectance and transmittance are similar to those of OLD1.

The TOC simulations are presented in Fig. 3. Before analysing the model performance, one can note the presence of a peak at 761 nm (band 15) in the CHRIS reflectance signatures, which corresponds with one of the oxygen absorption bands. This might be due to a spectral shift of the associated CHRIS band. Fig 3. shows a good match between SLC simulations and CHRIS data especially for the YOUNG and OLD1 stand. The OLD2 stand is less well modelled. Small discrepancies appear in the blue and red bands where

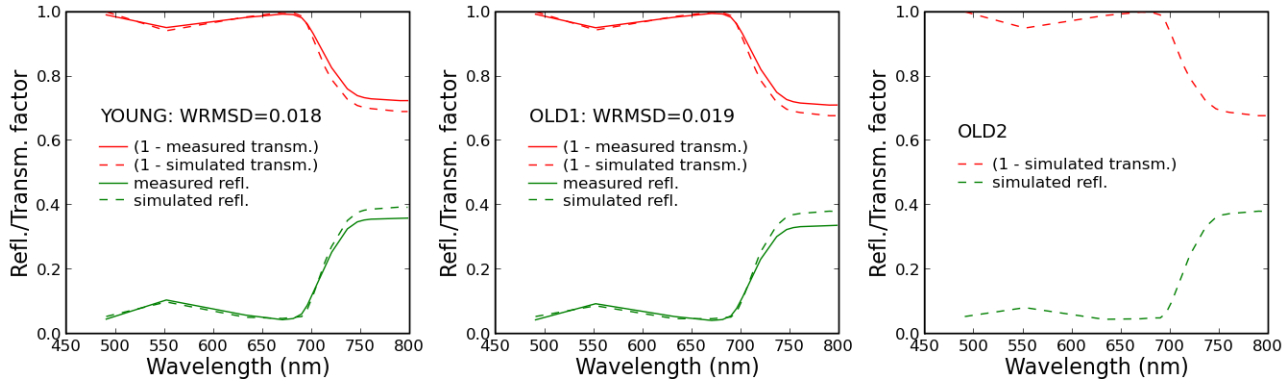

Figure 2. Measured and simulated needle reflectance and transmittance factors

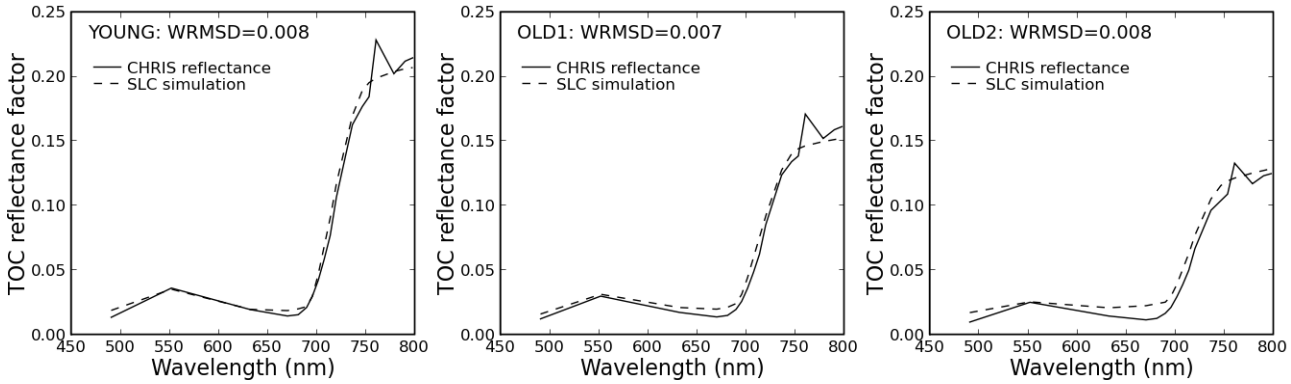

Figure 3. CHRIS atmospherically corrected and simulated TOC reflectance factor (r_{so})

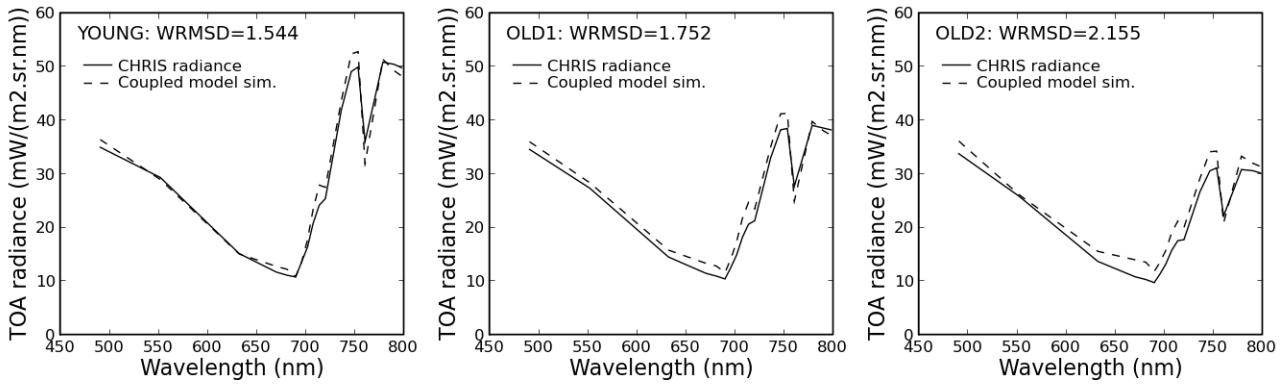

Figure 4. CHRIS and simulated TOA radiance (L_o)

the simulations are slightly too high. Another small difference is the more rounded NIR shoulder in the simulations than in the CHRIS data.

A good match between the simulations of the coupled model and the CHRIS radiance data was also obtained at TOA level. The TOA results are poorer for OLD2. The overall tendency is to overestimate the radiance, except for the dip at 761 nm where the simulations are lower. The 2 peaks around this dip present opposite trends in the CHRIS and simulated signature: in CHRIS, the 1st peak is lower than the 2nd one whereas it is the other way around for the simulations (Fig. 4).

3.2. Problem dimensionality and local sensitivity analysis

The histogram of the singular values for the YOUNG stand at TOA level (Fig. 5) shows that the singular values decrease with the singular value number. The histograms for the other 2 stands and also at TOC levels (not shown) look similar to Fig. 5. The main differences between TOC and TOA histograms were the number of singular values (15 at TOC, the number of parameters; 18 at TOA, the number of wavelengths) and the magnitude of the singular values which was higher at TOC (1st value reached about 1.6) than at TOA (1st value reached about 1.2). In the 6 cases, the rank of the singular matrix was taken at 3. This means

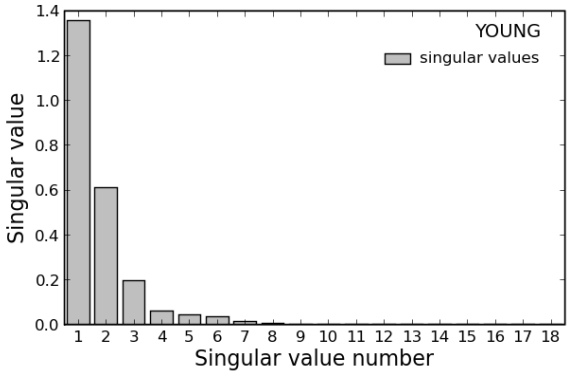

Figure 5. Singular values obtained at TOA level for the YOUNG stand

that the rank of the estimation problem is 3 and that a maximum of 3 parameters can mathematically be estimated.

Therefore, the first 3 axes of the transformed parameter variations space were further investigated. Absolute values were used because the signs of the loadings are arbitrary. The bigger the absolute value, the more influential the parameter is. At TOC level (Fig. 6), the loadings are quite similar for YOUNG and OLD1 and slightly different for OLD2. It was, however, possible to distinguish most important parameters for each axis that are common to the 3 stands. These were: Cv, needle Cdm, and needle Cab for axis 1; needle Cab, fB, and needle Cdm for axis 2; and needle Cab, fB, and Cv for axis 3.

At TOA level (Fig. 7), the situation regarding the SLC parameters is comparable to that at TOC level. Additional information was also obtained about the atmospheric parameters. Surface height and visibility are the most influential atmospheric parameters, but they only appear in the 2nd and 3rd axes and are much less important than Cv, fB, needle Cab, and needle Cdm. The water vapour and the ozone have very little influence and the surface temperature has no influence at all. One of the most remarkable outcomes is the insensivity to LAI, which implies that LAI is very hard to estimate for these dense forest stands.

Overall, the most influential parameters for the 3 stands at both TOC and TOA level were: Cv, fB, needle Cab, and needle Cdm. Although the rank was 3, all 4 parameters were left free in the LUTs because they are common to the 3 stands and it is not obvious which 3 parameters are most influential among these 4.

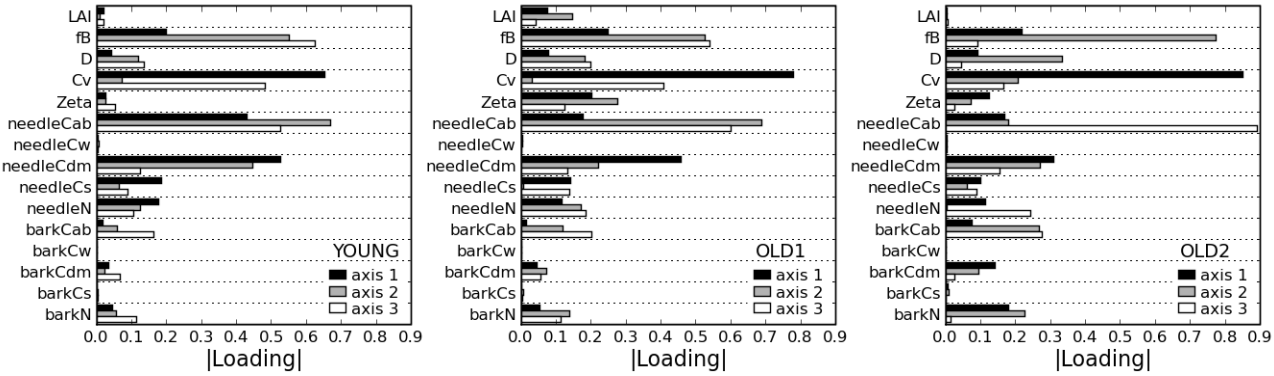

Figure 6. Absolute values of the parameter loadings obtained at TOC level

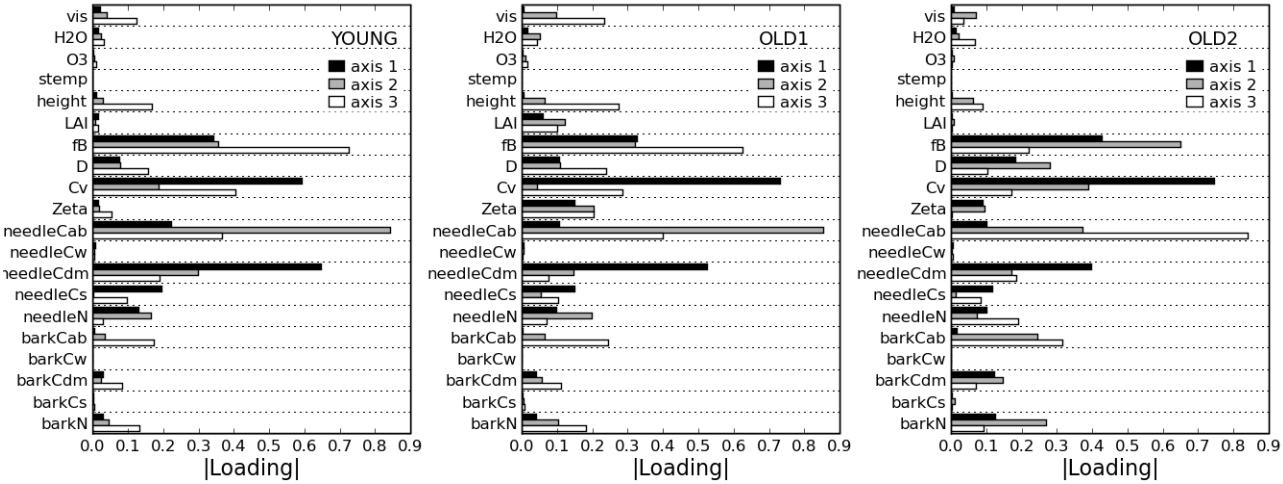

Figure 7. Absolute values of the parameter loadings obtained at TOA level

3.3. Parameter estimation

The estimates obtained from TOC and TOA level for the 3 stands are presented in Tab 4. In all cases the estimation problem had only 1 solution, except for OLD1 at TOC level where there were 2 solutions; so it seems that full coupling set up of the TOA approach was efficient in decreasing the ill-posedness at least for this case. The WRMSD of the solutions have the same order of magnitude as those of the simulations (Fig. 3 and 4) but are smaller. For the 3 stands, the estimates obtained from TOC and TOA level have similar values. Comparing with the values used in the simulations (Tab. 1), the estimates from TOA level were better for YOUNG and OLD2, whereas the estimates from TOC level were better for OLD1. Regarding the parameters, Cv was more accurately estimated than the other 3 parameters.

Table 4. Estimates of fB, Cv, needle Cab (μg/cm^2), and needle Cdm (g/cm^2) obtained for the 3 stands at TOC and TOA levels

Stand	YOUNG		OLD1		OLD2	
Level	TOC	TOA	TOC	TOA	TOC	TOA
WRMSD	0.007	1.4	0.005	1.1	0.006	1.7
# solutions	1	1	2	1	1	1
fB	0	0	0	0	0.3	0.4
Cv	0.7	0.8	0.6	0.6	0.7	0.7
Needle Cab	55	55	77.5	80	100	95
Needle Cdm	0.03	0.04	0.05	0.05	0.05	0.05

4. DISCUSSION

Although the PROSPECT inputs could be optimized to nicely simulate needles and bark, one cannot expect that the estimates obtained for the needle parameters match reality because PROSPECT does not work well for needles (the measured Cab values were around 40 μg/cm2 and Cdm around 0.015 g/cm2). This could be solved by recalibrating the optical coefficients for needles as proposed by [14].

The TOC simulations matched the atmospherically corrected CHRIS data well, despite the absence of branch and shoot level clumping in 4SAIL2. Also at TOA level the simulations compared well with the CHRIS data. In both case, the tendency was towards overestimation. This is unlikely to be due to neglecting the adjacency effect because most of the CHRIS scene was covered by forest. The TOC and TOA simulations were less good for the OLD2 stand, which may be related to its field data which was less complete and of less quality.

Similar to [15], the SVD of the Jacobian matrix proved very useful for helping with the parameter estimation by indicating the actual rank of the problem and pointing out the most influential parameters which can be estimated. These were: Cv, fB, needle Cab and Cdm, which are useful parameters for biomass estimation for e.g. climate and fire applications.

The estimates obtained from TOC and TOA level were similar and were most accurate for the Cv parameter. Neither approach was best for all stands. The estimation step made use of all knowledge gained from the field campaign and simulation step. It would be worth investigating the performance of the estimations in realistic settings where many data are unknown.

This study extends to a forest case study the results of [15] who successfully estimated the brown leaf parameters and LAI, LIDF a and b, and hot, for a mixed canopy of low LAI with the same SLC and MODTRAN coupled model using hyperspectral-multidirectional simulated SPECTRA data.

This study showed that the TOA approach performed as good as the traditional TOC approach for estimating needle and canopy parameters and that the full model coupling set up used in the TOA approach was successful in decreasing the ill-posedness for at least one stand. In addition, the TOA approach presents a number of advantages over the TOC approach.

First of all, it avoids the atmospheric correction step which is an inversion problem in itself and requires simplifying assumptions such as surface Lambertianity. This can be well seen in Eq. 2 and 12: Eq. 2 (canopy-atmosphere coupling) has 7 parameters whereas Eq. 12 (atmospheric correction) has only 3.

Second, the output of the coupled model is a physical quantity which is actually measured by the satellite, so that the comparison between model output and satellite data is direct and straightforward. In the TOC approach, on the other hand, the canopy model produces the bidirectional reflectance factor, whereas the atmospherically corrected satellite data are hemispherical-directional reflectance factors, and it is usually assumed that these 2 quantities are similar.

Because the atmosphere model is used in forward mode in the TOA approach, one can more easily include canopy directional effects, adjacency effect, and terrain topography effects to obtain a realistic description of the atmospheric effects.

The TOA approach allows fully exploiting the model coupling regularization method, and the other methods can be used in addition: it is still possible to include prior information and to enforce spatial and temporal constraints when working at TOA level.

From an operational point of view, the TOA approach facilitates data assimilation and the use of multi-sensor data because minimal pre-processing of the data is needed.

5. CONCLUSION

The SLC model and the SLC-MODTRAN coupled model were successfully used to simulate respectively TOC reflectance and TOA radiance of three Norway spruce stands as measured by CHRIS. The SVD of the Jacobian matrix was a powerful tool to diagnose the

rank of the parameter estimation problem and the influence of each model input parameter both at TOC and TOA level. A LUT was used to estimate Cv, fB, needle Cab and needle Cdm. The most accurate estimates were obtained for Cv, but neither TOC or TOA approach performed best for all 3 stands. The TOA approach allowed decreasing the ill-posedness for at least one stand.
Further research will make use of the multi-angular capabilities of CHRIS/PROBA and investigate the potential of the images with other viewing directions to improve the performance of the parameter estimations.

6. ACKNOWLEDGEMENT

The data collection was conducted under ESA/PECS project No. 98029 and kindly provided by the Institute of Systems Biology and Ecology, Academy of Sciences of the Czech Republic. The authors wish to thank Petr Lukeš and Lucie Homolová for their help with the data and Allard de Wit for his assistance with model implementation and LUTs.

7. REFERENCES

1. Baret F. & Buis S. (2008). Estimating Canopy Characteristics from Remote Sensing Observations: Review of Methods and Associated Problems. In Advances in Land Remote Sensing: System, Modeling, Inversion and Application (Eds. S. Liang), Springer, pp 173-201.

2. Verhoef W. & Bach H. (2003). Remote Sensing Data Assimilation Using Coupled Radiative Transfer Models. *Phys. Chem. of Earth*. **28**(1-3), 3-13.

3. Verhoef W. & Bach H. (2007). Coupled Soil-Leaf-Canopy and Atmosphere Radiative Transfer Modeling to Simulate Hyperspectral Multi-Angular Surface Reflectance and Toa Radiance Data. *Rem. Sen. of Env.* **109**(2), 166-82.

4. Berk A., Anderson G.P., Acharya P.K., *et al.* (2003). Modtran4 Version 3 Revision 1 User's Manual, Airforce Research Laboratory, Hanscom, MA, USA, pp 97.

5. Verhoef W. & Bach H. (2003). Simulation of Hyperspectral and Directional Radiance Images Using Coupled Biophysical and Atmospheric Radiative Transfer Models. *Rem. Sen. of Env.* **87**(1), 23-41.

6. Bach H. & Verhoef W. (2009). Sentinel-3 Land Scene Generator for Optical System Performance Simulator, VISTA Geowissenschaftliche Fernerkundung GmbH, pp 59.

7. Kratochvilová I., Janouš D., Marek M., Barták M. & Řiha L. (1989). Production Activity of Mountain Cultivated Norway Spruce Stands under the Impact of Air Pollution. I. General Description of Problems. *Ekológia*. **8**(4), 407-19.

8. Marek M.V., Malenovský Z., Homolová L., Hanuš J., Kaplan V. & Lukeš P. (2007). Spectral-Spatial Scaling from Leaf to Canopy Level Using Spectro-Directional Approaches in Support of the Gmes Sentinel 2: 'Superspectral' Mission - 3rd Esa/Pecs Project Report for Period of January 1st 2007 – December 31st 2007, Institute of Systems Biology and Ecology, Academy of Sciences of the Czech Republic (ISBE ASCR), pp 27.

9. Lukeš P. (2009). Personal communication. Institute of Systems Biology and Ecology, Academy of Sciences of the Czech Republic, Na Sádkách 7, 370 05, České Budějovice, Czech Republic.

10. Chen J.M. (1996). Optically-Based Methods for Measuring Seasonal Variation of Leaf Area Index in Boreal Conifer Stands. *Agric. For. Meteo.* **80**(2-4), 135-63.

11. Homolová L., Malenovský Z., Hanuš J., Tomášková I., Dvořáková M. & Pokorný R. (2007). Comparison of Different Ground Techniques to Map Leaf Area Index of Norway Spruce Forest Canopy. In Proc. '10th ISPMSRS' (Eds. M.E. Schaepman, S. Liang, N.E. Groot & M. Kneubühler), Intl. Archives of the Photogrammetry, Remote Sensing and Spatial Information Sciences.

12. Pokorný R. & Marek M.V. (2000). Test of Accuracy of Lai Estimation by Lai-2000 under Artificially Changed Leaf to Wood Area Proportions. *Biologia Plantarum*. **43**(4), 537-44.

13. Jacquemoud S. & Baret F. (1990). Prospect: A Model of Leaf Optical Properties Spectra. *Rem. Sen. of Env.* **34**(2), 75-91.

14. Malenovský Z., Albrechtová J., Lhotáková Z., *et al.* (2006). Applicability of the Prospect Model for Norway Spruce Needles. *Int. Journ. Rem. Sen.* **27**(24), 5315-40.

15. Verhoef W. (2007). A Bayesian Optimisation Approach for Model Inversion of Hyperspectral-Multidirectional Observations: The Balance with a Priori Information. In Proc. '10th ISPMSRS' (Eds. M. Schaepman, S. Liang, N. Groot & M. Kneubühler), Intl. Archives of the Photogrammetry, Remote Sensing and Spatial Information Sciences.